ACS APPLIED MATERIALS & INTERFACES

www.acsami.org

Research Article

Electrochemical DNA Sensors Based on MoS_2-AuNPs for Polynucleotide Kinase Activity and Inhibition Assay

Meihua Lin, Hao Wan, Jian Zhang, Quan Wang, Xinyu Hu, and Fan Xia*

Cite This: *ACS Appl. Mater. Interfaces* 2020, 12, 45814–45821

Read Online

ACCESS | Metrics & More | Article Recommendations | Supporting Information

ABSTRACT: The determination of T4 polynucleotide kinase (PNK) activity and the screening of PNK inhibitors are critical to disease diagnosis and drug discovery. Numerous electrochemical strategies have been developed for the sensitive measurement of PNK activity and inhibition. However, they often suffer from additional labels and multiple steps of the detection process for the electrochemical readout. Herein, we have demonstrated an electrochemical DNA (E-DNA) sensor for the one-step detection of PNK with "signal-on" readout with no need for additional labels. In our design, the highly switchable double-stranded DNA (dsDNA) probes are immobilized on the gold nanoparticle-decorated molybdenum disulfide nanomaterial (MoS_2-AuNPs), which possesses large surface area and high conductivity for elevating the signal gain in the PNK detection. This signal-on E-DNA sensor integrated with MoS_2-AuNPs exhibits a much higher sensitivity than that without MoS_2-AuNPs, showing a detection limit of 2.18×10^{-4} U/mL. Furthermore, this assay shows high selectivity, with the ability to discriminate PNK from other enzymes and proteins, and can be utilized to screen inhibitors. The proposed sensor is easy to operate with one-step readout and robust for PNK detection in the biological matrix and shows great potential for point-of-care in clinical diagnostics and drug screening.

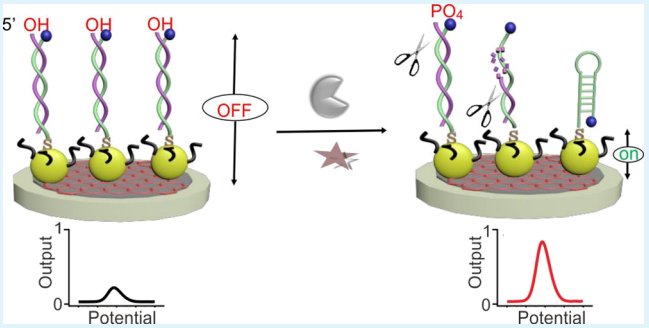

KEYWORDS: *electrochemical, biosensor, nanomaterial, polynucleotide kinase activity, one-step detection*

INTRODUCTION

PNK is a vital element of 5′-kinase family that can catalyze the transfer of the γ-phosphate residue from an adenosine triphosphate (ATP) to the 5′-hydroxyl terminus of DNA or RNA.[1,2] The abnormal activity of PNK would disturb the cellular responses to DNA damage and lesions, which is related to a variety of human diseases.[3−6] In addition, PNK inhibitors are promising drugs because the downregulation of PNK increases the sensitivity of cells to γ-radiation.[7] Therefore, the determination of PNK activity and inhibition has profound meanings in the biological research and clinical diagnosis. The traditional detection strategies for PNK activity including polyacrylamide gel electrophoresis (PAGE), radical isotope P-labeling, and autoradiography have been commonly used in biological experiments due to their accurate quantification.[8−10] However, the applications of these methods are limited by their laborious, complicated, and radioactive operations. To overcome these drawbacks, many approaches such as fluorescence,[11−18] colorimetric,[19] bioluminescence,[20] and electrochemical assays[21−24] have been developed. Among them, electrochemical assays have attracted increasing attention due to their obvious advantages of low cost, easy miniaturization, high sensitivity, and fast response.[25−28] Zhang et al. constructed an electrochemical biosensor for the determination of PNK with a detection limit of 0.0027 U/mL by phos-tag-biotin-mediated alkaline phosphatase catalytic amplification.[29] To improve sensitivity, several nanomaterials have been introduced in electrochemical sensors. Zhang's group and Luo's group, separately, developed an electrochemical detection method of PNK, based on iron metal−organic framework-loaded gold nanoparticles to improve the sensitivity.[22,30] Cui et al. employed gold nanoparticles as carriers to enhance the signal, which can detect PNK as low as 7.762×10^{-4} U/mL.[31] Although great achievements for PNK assay have been made, the additional label of nanomaterials for generating signals in these approaches may restrict their broader applications, such as real-time monitoring enzymatic reactions. Therefore, the development of more simple and facile methods with less steps for determination of PNK is still desired.

The E-DNA sensor was first reported by Fan in 2003[32] and then has attracted substantial attention due to its fast response and single-step detection of targets directly in complex

Received: July 25, 2020
Accepted: September 2, 2020
Published: September 2, 2020

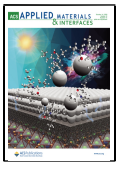

https://dx.doi.org/10.1021/acsami.0c13385
ACS Appl. Mater. Interfaces 2020, 12, 45814–45821

matrices.[33−36] The archetype of the E-DNA sensor comprises a hairpin structure dually modified with a redox reporter for signal output and a thiol for probe immobilization.[32] Binding of the target to the hairpin structure largely changes its conformation as the linear structure, which makes the reporter far away from the interrogating electrode, producing a target-depending reduction in the redox current. The target-induced conformational change of this signal transduction mechanism enables the application of the E-DNA sensor in clinical samples and real-time monitoring of the recognition process with reagentless procedures and single-step convenience. After this, many signal-on E-DNA sensors have been constructed to circumvent the limitations of the first signal-off E-DNA sensor where the maximal signal gain is no more than 100%.[37−41] The signal-on E-DNA sensors not only have the advantages of single-step detection of targets directly in complex matrices but also improve signal gain and sensitivity. Therefore, the signal-on E-DNA sensor provides a unique opportunity for the detection of PNK activity and inhibition with a single-step convenience and excellent performance.

Herein, motivated by these observations, we designed a new signal-on E-DNA sensor combined with MoS_2-AuNPs for one-step, sensitive, and selective analysis of PNK activity and inhibitor screening. The architecture of the E-DNA sensor is changed by the PNK-induced lambda exonuclease (λ exo) cleavage reaction, which in turn produces an increased signal. MoS_2-AuNPs have been widely exploited as an electrode-decorated material to improve the electrical conductivity for the ultrasensitive detection of small molecules, proteins, and nucleic acids.[42−47] The sensor has combined the advantages of the E-DNA sensors and MoS_2-AuNPs: (1) the E-DNA sensor is easy to use and enables the detection of PNK directly in complicated samples with high sensitivity, showing potential for clinical applications; (2) compared to the reported signal-off biosensor with a limitation of the maximal signal suppression, this E-DNA sensor generates a stable signal-on electrochemical signal; (3) the single-step and reagentless convenience and signal stability enable the sensor to monitor the activity of PNK in real time; (4) MoS_2-AuNPs can not only provide large area for immobilization, but also provide a good pathway of electron transfer for the electroactive reporter to enhance the faradaic current and improve the sensitivity for PNK assay. We have demonstrated that this E-DNA sensor can sensitively detect PNK in both buffer and cell lysate screen PNK inhibitors and can be further exploited for disease diagnostics and drug discovery.

EXPERIMENTAL SECTION

Materials and Instruments. All materials and instruments are provided in the Supporting Information.

Preparation of MoS_2-AuNPs. MoS_2 nanosheets, AuNPs, and MoS_2-AuNPs were synthesized according to the reported work,[48,49] and their syntheses are described in the Supporting Information.

Electrophoresis Analysis. For the formation of the dsDNA, 1 μM sDNA and its cDNA were first mixed at a ratio of 1.5:1 in the working buffer (70 mM Tris−HCl, 1 mM ATP, 10 mM $MgCl_2$, 5 mM DTT, pH 7.6). The mixture was heated at 95 °C for 5 min and then cooled to 4 °C. The prepared dsDNA was then incubated with 10 U/mL PNK and 10 U/mL λ exo (without PNK or λ exo as control groups) for 2 h at 37 °C. Afterward, the samples were analyzed by 16% native PAGE with a constant voltage of 85 V for 120 min. After staining with Gelred, the gel was photographed.

Fabrication of the Electrochemical Biosensor. A glassy carbon electrode (GCE) was first polished with 0.3 and 0.05 μm alumina slurry for 3 min, respectively. The GCE was then sonicated in ethanol and Milli-Q water for 5 min, respectively. After being rinsed with Milli-Q water and dried with nitrogen gas, the GCE was incubated with 5 μL of the as-prepared MoS_2-AuNPs for 12 h at room temperature. Then, 5 μL of the prepared dsDNA was dropped on the MoS_2-AuNPs/GCE and assembled for different time periods at room temperature, forming dsDNA/MoS_2-AuNPs/GCE. Following this, the dsDNA/MoS_2-AuNPs/GCE was incubated with 2 mM 6-mercaptohexanol (MCH) for 2 h. The working electrode was measured by electrochemical impedance spectroscopy (EIS) after each modified step. The control experiments were performed in the same process except for the first step. For the E-DNA sensor on the gold electrode, the first step was to clean the electrode, as described previously.[50,51]

Measurement of PNK Activity, Stability, and Kinetics. After being rinsed with PBS, the MCH/dsDNA/MoS_2-AuNPs/GCE was incubated with the working buffer containing different-concentration PNK at 37 °C for different time periods. We optimized the concentration of ATP and λ exo and the incubation time. After reaction, the electrodes were subjected to cyclic voltammetry (CV) and square wave voltammetry (SWV) measurements in MB buffer. For studying the stability, the electrodes before and after incubation with PNK were monitored by SWV for 1 h at an interval of 3 min. For studying the lifetime, the electrodes after incubation with PNK were continually monitored by SWV for 132 h at an interval of 12 h. For the measurement of PNK kinetics, the MCH/dsDNA/MoS_2-AuNPs/GCE was immersed in the optimized working buffer containing 1 U/mL PNK and monitored by SWV.

Preparation of Cell Lysates. HeLa cells were cultured in DMEM supplemented with 10% fetal bovine serum and 1% penicillin−streptomycin and incubated with 5% CO_2 at 37 °C. HeLa cells were collected with trypsinization and washed twice with PBS. After resuspending in Tris−HCl buffer, the cells were counted and frozen at −80 °C and thawed at room temperature for 3 cycles. After removing the cell fragments, the supernatant was stored at −80 °C. Diluted cell extracts were added to the assay solution (50%). The MCH/dsDNA/MoS_2-AuNPs/GCE was incubated with the diluted cell extracts containing different-concentration PNK (0−10 U/mL) at 37 °C for 3 h.

Inhibition Assay. ADP, NaH_2PO_4, and $(NH_4)_2SO_4$ were used as the model inhibitors for PNK. The inhibitors with different concentrations were incubated with 1 U/mL PNK in the optimized working buffer with the same procedures, as described above.

RESULTS AND DISCUSSION

Principle of the Proposed Biosensor. For investigating PNK with high sensitivity in a single-step readout, we decorated the E-DNA sensor on the MoS_2-AuNP-modified GCE (Scheme 1). A hairpin DNA with 5′-OH as the substrate DNA (sDNA, −7.18 kcal/mol, free energy of the secondary structure) for PNK is first prehybridized with its complementary DNA (cDNA, −11.22 kcal/mol) dually modified with

Scheme 1. Schematic Illustration (Not to Scale) of the Signal-on E-DNA Sensor for the Detection of PNK Activity

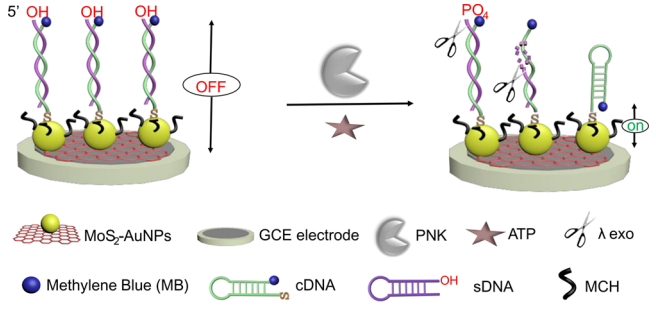

https://dx.doi.org/10.1021/acsami.0c13385
ACS Appl. Mater. Interfaces 2020, 12, 45814−45821

5′-thiol and 3′-methylene blue (MB) for immobilization and signaling, respectively. The formation of the dsDNA (−35.84 kcal/mol) is thermodynamically more favorable (Figure S1, Supporting Information). The dsDNA is first immobilized on the MoS_2-AuNP-modified GCE via the Au−S bond. Notably, the dsDNA with a relatively rigid structure keeps the distal MB away from the electrode surface, limiting the electron transfer. The λ exo-mediated cleavage reaction cannot occur without PNK because of the lack of 5′-phosphoryl; hence, MB is maintained on the distal end, generating a low background current. λ exo is a highly processive 5′ to 3′ dsDNA exonuclease to digest the 5′-phosphorylated strand.[52] Therefore, after being phosphorylated by PNK, sDNA is further cleaved by λ exo to liberate the cDNA from the dsDNA. Subsequently, the free cDNA switches to its intrinsic hairpin structure to make MB close to the electrode surface, which can efficiently transfer electrons to the surface and increase the redox current. That is to say, by combining PNK phosphorylation with the λ exo cleavage reaction, the conformation of the E-DNA sensor is changed and a signal-on readout is produced. In addition, MoS_2-AuNPs providing large area and good conductivity for the efficient electron transfer of MB can greatly improve the sensitivity of the E-DNA sensor for PNK detection.

Characterization of MoS_2-AuNPs. The morphologies of the prepared MoS_2 nanosheets and MoS_2-AuNP nanomaterials were characterized by TEM. As shown in Figure 1A, the exfoliated MoS_2 nanosheets were thin with multilayers (inset), and AuNPs dispersed on their surface after $AuCl_4^-$ were mixed and reduced by MoS_2, indicating the successful synthesis of MoS_2-AuNPs. The sizes of AuNPs were almost uniform around 20 nm (Figure 1B). Ultraviolet−visible (UV−vis) spectroscopy was also employed to confirm the formation of MoS_2-AuNPs. As shown in Figure 1C, compared to MoS_2 nanosheets, a new absorption peak at around 540 nm was observed in the MoS_2-AuNP nanomaterial, corresponding to the absorption of gold nanoparticles. Moreover, the solution color changed from yellow-brown to purple (photograph in the inset of Figure 1C) after MoS_2 nanosheets reacted with $AuCl_4^-$. These results demonstrate that MoS_2-AuNPs have been successfully synthesized.

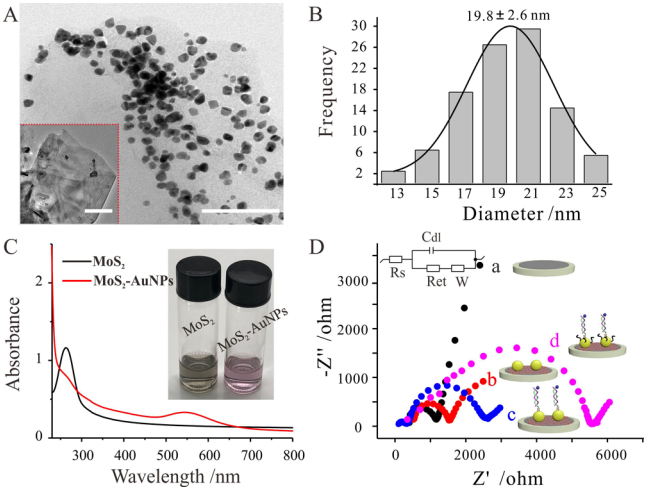

Figure 1. Characterization of nanomaterials and modified electrode. (A) Typical TEM images of MoS_2 nanosheets (inset) and MoS_2-AuNPs. Scale bar: 100 nm. (B) Size distribution of AuNPs that are decorated on the surface of MoS_2 nanosheets. (C) UV−vis absorption spectra and photographs (inset) of MoS_2 nanosheets and MoS_2-AuNPs. (D) Nyquist plots of EIS for stepwise fabrication: (a) bare GCE, (b) MoS_2-AuNPs/GCE, (c) dsDNA/MoS_2-AuNPs/GCE, and (d) MCH/dsDNA/MoS_2-AuNPs/GCE. The inset shows the Randles equivalent circuit used to fit the EIS data.

Characterization of the Modified Electrode. After successfully synthesizing MoS_2-AuNPs, we employed EIS to verify the stepwise fabrication of the MoS_2-AuNP-based E-DNA sensor that was performed in $[Fe(CN)_6]^{3-/4-}$. The EIS results were fitted to the Randles equivalent circuit, which contained the electron transfer resistance (R_{et}), the solution resistance (R_s), the Warburg impedance (W), and the double layer capacitance (C_{dl}) (inset in Figure 1D). The semicircle diameter of the Nyquist plot was used to reflect the R_{et}.[53] As shown in Figure 1D, after incubation with MoS_2-AuNPs, the semicircle slightly increased (curve b) in comparison with the bare GCE (curve a), due to the negative surface charge of the nanomaterials (Figure S2) impeding the diffusion of ferricyanide, implying the MoS_2-AuNPs were successfully modified on the surface of the GCE. After the assembly of the prehybridized dsDNA on the MoS_2-AuNPs/GCE (curve c), the semicircle continuously enhanced because the negatively charged DNA phosphate backbone had an electrostatic repulsion with the negatively charged $[Fe(CN)_6]^{3-/4-}$, demonstrating the successful modification of the DNA. Then, the introduction of nonconductive MCH replaced the nonspecific adsorption of the DNA and blocked the residual active spots, further inhibiting the diffusion of ferricyanide, and the semicircle diameter became larger. Therefore, the changes in EIS data indicate the successful fabrication of the E-DNA sensor on the MoS_2-AuNPs/GCE.

Feasibility of PNK Assay. To demonstrate the feasibility of our method, the enzymatic reactions in solution were first verified through native PAGE. As shown in Figure 2A, the

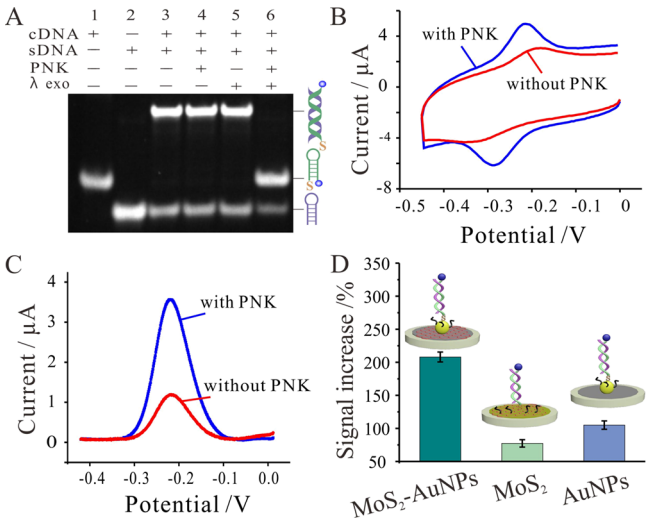

Figure 2. Feasibility verification by gel electrophoresis and electrochemical analysis. (A) 16% native PAGE analysis. The ratio of sDNA/cDNA was 1.5:1 in lanes 3−5. Typical CV (B) and SWV (C) responses of the MoS_2-AuNP-based E-DNA sensor in the absence (red) and presence (blue) of 0.1 U/mL PNK, respectively. (D) Signal increase produced by the MoS_2-AuNP-based E-DNA sensor was significantly enhanced, compared to the same E-DNA sensors decorated on the surface of the MoS_2/gold electrode and AuNPs/GCE in response to 0.1 U/mL PNK.

https://dx.doi.org/10.1021/acsami.0c13385
ACS Appl. Mater. Interfaces 2020, 12, 45814−45821

bands in lane 1 and lane 2 represented cDNA and sDNA, respectively. A new band with a slower mobility appeared after cDNA was mixed with sDNA at a ratio of 1:1.5 (lane 3), indicating that cDNA completely hybridized with sDNA to form the dsDNA with excess sDNA. In the presence of both PNK and λ exo (lane 6), the band of the dsDNA disappeared and a new band corresponding to cDNA formed, suggesting that the phosphorylated dsDNA was degraded by λ exo to successfully release cDNA. Simultaneously, the band of sDNA in lane 6 became weaker than that in lanes 3−5, demonstrating that free sDNA can form a hairpin structure and be digested by λ exo after phosphorylation. However, without λ exo (lane 4) or PNK (lane 5), the bands of the dsDNA and the excess sDNA remained intact, and the band of cDNA was not observed. Therefore, PAGE assay confirmed that the dsDNA with 5′-OH can be phosphorylated by PNK and then cleaved by λ exo to release cDNA.

Then, CV and SWV measurements were carried out to investigate the sensing feasibility of the E-DNA sensor on the surface of MoS_2-AuNPs. As shown in Figure 2B, when PNK was absent, we observed a pair of small characteristic redox peaks of MB, indicating the successful electron transfer. The small peaks are possibly caused by the rigidity of the dsDNA, which limits the accessibility of the terminal MB to the electrode surface, hindering the efficient electron transfer. We found that this peak pair apparently increased after the addition of PNK, suggesting that the electron transfer became more efficient. We speculate that sDNA is phosphorylated by PNK and digested by λ exo, thereby enabling the dsDNA to release the cDNA. In this case, the free cDNA switches to its intrinsic hairpin structure to make MB close to the electrode surface, inducing an increase electrochemical signal. SWV was then employed to directly quantify the electrochemical response. A representative and relatively small SWV peak at around −0.2 V was observed in the absence of PNK (Figure 2C). In contrast, a prominently enhanced peak current was obtained in the presence of PNK. These results confirmed that the E-DNA sensor is available for PNK assay. Moreover, the signal increase of our MoS_2-AuNP-based E-DNA sensor was about 208% and the corresponding signal gains of the same E-DNA sensor decorated on the AuNPs/GCE and MoS_2/gold electrode were about 77 and 105% (Figure 2D), respectively. This is presumably attributed to the synergic effects between AuNPs and MoS_2 nanosheets, such as providing a large area and excellent conductivity for efficient electron transfer. Therefore, MoS_2-AuNPs can enhance the signal gain of the E-DNA sensor, which is beneficial for improving the sensitivity.

Stability, Kinetics, Selectivity, and Robustness of the MoS_2-AuNP-Based E-DNA Sensor. Under the optimal experimental conditions (3 h immobilization, 20 U/mL λ exo, 1 mM ATP, and 3 h enzymatic reaction, Figure S3), the stability of the MoS_2-AuNP-based E-DNA sensor was evaluated by scanning SWV repeatedly. The SWV peak currents obtained from 21 cycles almost remained consistent with each other both in the absence and presence of PNK (Figure 3A and Figure S4B). The peak currents under both states fluctuated within ±1% in comparison with the mean currents over 1 h (Figure S4A). Notably, when the sensor was monitored for several days, we found the SWV peak currents reduced with an increase in the test time (Figure S5). We speculate that the nonspecific adsorption of MoS_2-AuNPs on the GCE is not robust enough and detached from the surface when the electrodes were immersed in buffer solution for a

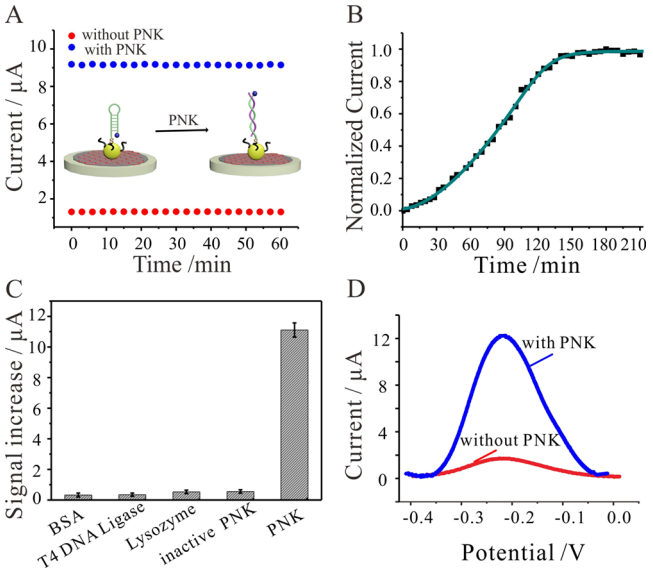

Figure 3. (A) SWV peak currents of the MoS_2-AuNP-based E-DNA sensor under states of without (red) and with 0.1 U/mL PNK (blue) monitored continually for 1 h in an interval of 3 min. (B) Monitoring the enzymatic reactions at 37 °C for more than 3 h with 1 U/mL PNK. (C) Specificity test of the sensor. The concentrations of all enzymes were 10 U/mL, and 10 nM BSA was used in the experiments. (D) Typical CV responses of the MoS_2-AuNP-based E-DNA sensor in cell lysate without (red curve) and with 10 U/mL PNK (blue curve).

long time. However, our sensor showed an average 10% reduction in the initial currents when tested for 12 h, which is sufficient for the detection of common biomolecules. These results demonstrate that the electron transfer of the MoS_2-AuNP-based E-DNA sensor is stable and reliable for PNK assay.

Then, taking advantage of the single-step readout and stable signal output, we monitored the enzymatic reactions in real time. The signal increased with an increase in the reaction time and saturated at about 150 min (Figure 3B), which was consistent with the results of the optimizing reaction time (Figure S3). Interestingly, the reaction rate was very slow at the initial 40 min and then increased before reaching the equilibrium. We speculate that although the relatively high density of the dsDNA at the initial state can increase the rate of phosphorylation,[54] the relatively narrow distance between neighboring probes may make the digestion of λ exo difficult and slow. Therefore, the sensor for PNK detection shows slower response than that for DNA detection.[37]

Next, to investigate the selectivity of the method, some proteins containing BSA, T4 DNA ligase, lysozyme, and heat-inactive PNK were chosen as the nonspecific interference. Compared with the blank sample, only PNK produced a remarkable increase in the electrochemical current, while other proteins and enzymes generated negligible current increase (Figure 3C). This result demonstrates that only phosphorylated dsDNA can be specifically degraded by λ exo to release cDNA for signal enhancement. Therefore, our method is highly specific for PNK detection.

Furthermore, to investigate the robustness of the MoS_2-AuNP-based E-DNA sensor, we tested the response in the HeLa cell lysate as a mold of complex matrix. As shown in Figure 3D, a typical SWV peak was obtained, indicating the feasibility of the electron transfer of the sensor in the cell

https://dx.doi.org/10.1021/acsami.0c13385
ACS Appl. Mater. Interfaces 2020, 12, 45814−45821

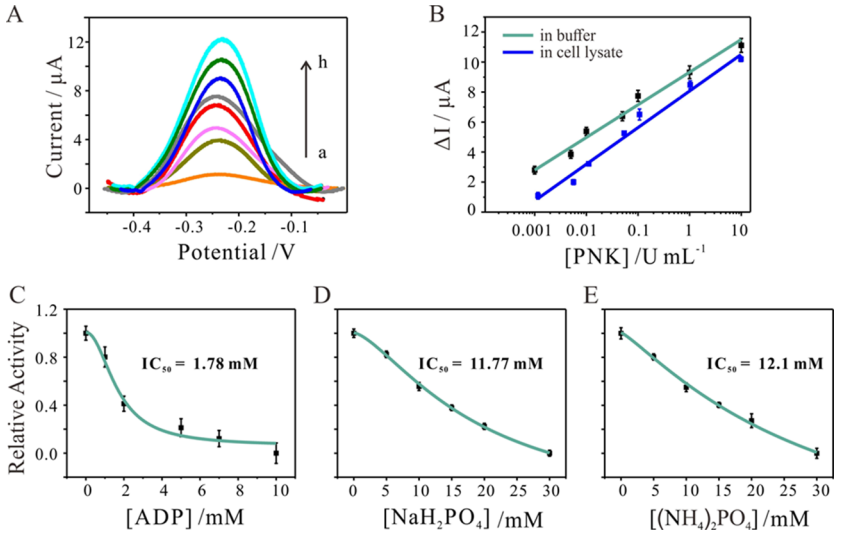

Figure 4. (A) SWV curves for PNK detection with different concentrations (a–h): 0, 0.001, 0.005, 0.01, 0.05, 0.1, 1, 10 U/mL, respectively. (B) Dependence of ΔI on the logarithm of PNK concentration in buffer (cyan) and cell lysate (blue). The effects of different inhibitors (C) ADP, (D) Na_2HPO_4, and (E) $(NH_4)_2SO_4$ on PNK activity. The error bars represent the standard deviation of three independent experiments.

lysate. The peak current significantly increased in the presence of PNK, as observed in pure buffer. These results demonstrate that the proposed sensor is robust and feasible for PNK analysis in complicated fluids.

Applications in Detection Sensitivity. Having substantiated the feasibility, stability, selectivity, and robustness of the MoS_2-AuNP-based E-DNA sensor for PNK assay, we further investigate the analytical sensitivity of the strategy. As shown in Figure 4A, the SWV signal increased as the concentration of PNK increased, demonstrating a great concentration-dependent current response for quantitative detection. The peak current increase (ΔI) was proportional to the concentration of PNK, which can be fitted with a Langmuir–Freundlich isotherm, demonstrating that the detection mechanism is based on the adsorption of PNK (Figure S6). The detailed relationship between the peak current increase (ΔI) and the logarithm of PNK concentration is summarized in Figure 4B (cyan line). A good linear range is from 0.001 to 10 U/mL, with the regression equation of $\Delta I = 2.176\lg c + 9.326$ (c represents the concentration of PNK) with $R^2 = 0.991$. The limit of detection is 2.18×10^{-4} U/mL, according to the criteria of $3\sigma/S$ (σ represents the standard deviation of the blank control and S is the slope of the fitting line shown in Figure 4B), which is lower than or comparable to other reported methods (Table S1).[11,30,31] We also calculated the limit of detection in different ways according to IUPAC recommendations, such as the rules of 3σ and 10σ (Table S2). As a control, when the E-DNA sensor was decorated on the gold electrode for PNK assay under the optimal conditions, ΔI was linearly proportional to the concentration of PNK in the range from 0.001 to 1 U/mL with a detection limit of 0.0013 U/mL (Figure S7), 6 times as high as that of the MoS_2-AuNP-based E-DNA sensor. These results indicate that MoS_2-AuNPs as substrates can significantly improve the sensitivity.

To investigate the practicability of the developed strategy, we further challenged the PNK detection in the HeLa cell lysate. As observed in pure buffer, ΔI also increased with an increase in PNK concentration (Figure S8), and exhibited a good linear correlation ($R^2 = 0.992$) with the regression equation of $\Delta I = 2.37\lg c + 8.14$ (Figure 4B, blue line). The limit of detection is estimated to be 0.0023 U/mL, demonstrating that the proposed sensor has great potential for clinical applications.

Inhibition Assay. Because inhibitors can enhance the efficacy of cancer treatment, the screening of the effective PNK inhibitors is significant for the development of clinical therapeutics. Thus, we selected three inhibitors in the reported work,[13] ADP, NaH_2PO_4, and $(NH_4)_2SO_4$, with no influence on λ exo activity, as models for inhibitor screening. ADP has a reverse impact on the phosphorylation reaction to inhibit the PNK activity, whereas NaH_2PO_4 and $(NH_4)_2SO_4$ inhibit the PNK activity by salt effects. The relative activity was calculated on the basis of $(1-I_i/I) \times 100\%$, where I_i and I are the SWV peak currents with and without inhibitors, respectively. As shown in Figure 4C–E, the relative activity decreased in response to the increasing concentrations of three inhibitors by fixing PNK at 1 U/mL, indicating that the activity of PNK has been inhibited. The half-maximal inhibition values (IC_{50}) of ADP, NaH_2PO_4, and $(NH_4)_2SO_4$ were 1.78, 11.77, and 12.1 mM, respectively, which are consistent with those in previous reports.[11,55,56] The result demonstrates that the proposed sensor can be used to screen PNK inhibitors.

CONCLUSIONS

In summary, we have developed a new signal-on E-DNA sensor integrated with MoS_2-AuNPs for PNK detection based on PNK-induced λ exo-degraded reaction for conformational change. Taking advantage of the large area and good conductivity of MoS_2-AuNPs and the highly switchable structure of the dsDNA probe for "signal-on" sensing, this sensor provided a detection limit of 2.18×10^{-4} U/mL in buffer and 0.0023 U/mL in the cell lysate. Due to its reagentless, stable, and single-step detection process, the E-DNA sensor can monitor the reaction and has the potential to quantify the kinetics of enzymatic reactions. In addition, this strategy was applied to estimate the inhibition effect of potential inhibitors, showing great potential in clinical diagnosis and drug screening.

https://dx.doi.org/10.1021/acsami.0c13385
ACS Appl. Mater. Interfaces 2020, 12, 45814–45821

■ ASSOCIATED CONTENT

Supporting Information

The Supporting Information is available free of charge at https://pubs.acs.org/doi/10.1021/acsami.0c13385.

Materials, instruments, the preparation process of nanomaterials; conformation and free energy of the secondary structure of DNA probes (Figure S1); zeta potential of MoS_2-AuNP nanomaterials (Figure S2),; optimization of experimental conditions (Figure S3); stability of the MoS_2-AuNP-based E-DNA sensor (Figures S4 and S5), Langmuir−Freundlich fitting (Figure S6), optimization, and sensitivity of the E-DNA sensor on the gold electrode surface (Figure S7); SWV peak current variation in buffer and cell lysates (Figure S6); comparison of different detection methods for PNK activity (Table S1); and calculation of the limit of detection (Table S2) (PDF)

■ AUTHOR INFORMATION

Corresponding Author

Fan Xia − *Engineering Research Center of Nano-Geomaterials of Ministry of Education, Faculty of Materials Science and Chemistry, China University of Geosciences, Wuhan 430074, China;* orcid.org/0000-0001-7705-4638; Email: xiafan@cug.edu.cn

Authors

Meihua Lin − *Engineering Research Center of Nano-Geomaterials of Ministry of Education, Faculty of Materials Science and Chemistry, China University of Geosciences, Wuhan 430074, China;* orcid.org/0000-0001-7616-7358

Hao Wan − *Engineering Research Center of Nano-Geomaterials of Ministry of Education, Faculty of Materials Science and Chemistry, China University of Geosciences, Wuhan 430074, China*

Jian Zhang − *Engineering Research Center of Nano-Geomaterials of Ministry of Education, Faculty of Materials Science and Chemistry, China University of Geosciences, Wuhan 430074, China*

Quan Wang − *Engineering Research Center of Nano-Geomaterials of Ministry of Education, Faculty of Materials Science and Chemistry, China University of Geosciences, Wuhan 430074, China*

Xinyu Hu − *Engineering Research Center of Nano-Geomaterials of Ministry of Education, Faculty of Materials Science and Chemistry, China University of Geosciences, Wuhan 430074, China*

Complete contact information is available at: https://pubs.acs.org/10.1021/acsami.0c13385

Notes

The authors declare no competing financial interest.

■ ACKNOWLEDGMENTS

This work is supported by the National Natural Science Foundation of China (21525523, 21974127, 21722507, 21574048, 21804122, and 21874121), the National Key R&D Program of China (2017YFA0208000), the Natural Science Foundation of Hubei Province of China (2018CFB169), the Fundamental Research Funds for the Central Universities, China University of Geosciences (Wuhan) (CUG170660), and the Open Project of State Key Laboratory of Supramolecular Structure and Materials (sklssm202018).

■ REFERENCES

(1) Richardson, C. C. Phosphorylation of nucleic acid by an enzyme from T4 bacteriophage-infected Escherichia coli. *Proc. Natl. Acad. Sci. U. S. A.* **1965**, *54*, 158−165.

(2) Novogrodsky, A.; Hurwitz, J. The enzymatic phosphorylation of ribonucleic acid and deoxyribonucleic acid. I. Phosphorylation at 5′-hydroxyl termini. *J. Biol. Chem.* **1966**, *241*, 2923−2932.

(3) Tahbaz, N.; Subedi, S.; Weinfeld, M. Role of polynucleotide kinase/phosphatase in mitochondrial DNA repair. *Nucleic Acids Res.* **2012**, *40*, 3484−3495.

(4) Reynolds, J. J.; Walker, A. K.; Gilmore, E. C.; Walsh, C. A.; Caldecott, K. W. Impact of PNKP mutations associated with microcephaly, seizures and developmental delay on enzyme activity and DNA strand break repair. *Nucleic Acids Res.* **2012**, *40*, 6608−6619.

(5) Garces, F.; Pearl, L. H.; Oliver, A. W. The structural basis for substrate recognition by mammalian polynucleotide kinase 3′ phosphatase. *Mol. Cell* **2011**, *44*, 385−396.

(6) Sharma, S.; Doherty, K. M.; Brosh, R. M., Jr. Mechanisms of RecQ helicases in pathways of DNA metabolism and maintenance of genomic stability. *Biochem. J.* **2006**, *398*, 319−337.

(7) Rasouli-Nia, A.; Karimi-Busheri, F.; Weinfeld, M. Stable down-regulation of human polynucleotide kinase enhances spontaneous mutation frequency and sensitizes cells to genotoxic agents. *Proc. Natl. Acad. Sci. U. S. A.* **2004**, *101*, 6905−6910.

(8) Bernstein, N. K.; Williams, R. S.; Rakovszky, M. L.; Cui, D.; Green, R.; Karimi-Busheri, F.; Mani, R. S.; Galicia, S.; Koch, C. A.; Cass, C. E.; Durocher, D.; Weinfeld, M.; Glover, J. N. M. The Molecular Architecture of the Mammalian DNA Repair Enzyme, Polynucleotide Kinase. *Mol. Cell* **2005**, *17*, 657−670.

(9) Lillehaug, J. R.; Kleppe, K. Kinetics and specificity of T4 polynucleotide kinase. *Biochemistry* **1975**, *14*, 1221−1225.

(10) Wang, L. K.; Shuman, S. Domain structure and mutational analysis of T4 polynucleotide kinase. *J. Biol. Chem.* **2001**, *276*, 26868−26874.

(11) Gao, M.; Guo, J.; Song, Y.; Zhu, Z.; Yang, C. J. Detection of T4 Polynucleotide Kinase via Allosteric Aptamer Probe Platform. *ACS Appl. Mater. Interfaces* **2017**, *9*, 38356−38363.

(12) Chen, F.; Zhao, Y.; Qi, L.; Fan, C. One-step highly sensitive florescence detection of T4 polynucleotide kinase activity and biological small molecules by ligation-nicking coupled reaction-mediated signal amplification. *Biosens. Bioelectron.* **2013**, *47*, 218−224.

(13) Lin, L.; Liu, Y.; Zhao, X.; Li, J. Sensitive and Rapid Screening of T4 Polynucleotide Kinase Activity and Inhibition Based on Coupled Exonuclease Reaction and Graphene Oxide Platform. *Anal. Chem.* **2011**, *83*, 8396−8402.

(14) Li, X.; Xu, X.; Song, J.; Xue, Q.; Li, C.; Jiang, W. Sensitive detection of T4 polynucleotide kinase activity based on multifunctional magnetic probes and polymerization nicking reactions mediated hyperbranched rolling circle amplification. *Biosens. Bioelectron.* **2017**, *91*, 631−636.

(15) Jin, T.; Zhang, J.; Zhao, Y.; Huang, X.; Tan, C.; Sun, S.; Tan, Y. Magnetic bead-gold nanoparticle hybrids probe based on optically countable gold nanoparticles with dark-field microscope for T4 polynucleotide kinase activity assay. *Biosens. Bioelectron.* **2020**, *150*, 111936.

(16) Wang, M.; Kong, D.; Su, D.; Liu, Y.; Su, X. Ratio fluorescence analysis of T4 polynucleotide kinase activity based on the formation of a graphene quantum dot−copper nanocluster nanohybrid. *Nanoscale* **2019**, *11*, 13903−13908.

(17) Feng, C.; Wang, Z.; Chen, T.; Chen, X.; Mao, D.; Zhao, J.; Li, G. A Dual-Enzyme-Assisted Three-Dimensional DNA Walking Machine Using T4 Polynucleotide Kinase as Activators and Application in Polynucleotide Kinase Assays. *Anal. Chem.* **2018**, *90*, 2810−2815.

(18) Ge, J.; Tang, L.-J.; Xi, Q.; Li, X.-P.; Yu, R.-Q.; Jiang, J.-H.; Chu, X. A WS2 nanosheet based sensing platform for highly sensitive detection of T4 polynucleotide kinase and its inhibitors. *Nanoscale* **2014**, *6*, 6866−6872.
(19) Jiang, H.-X.; Kong, D.-M.; Shen, H.-X. Amplified detection of DNA ligase and polynucleotide kinase/phosphatase on the basis of enrichment of catalytic G-quadruplex DNAzyme by rolling circle amplification. *Biosens. Bioelectron.* **2014**, *55*, 133−138.
(20) Du, J.; Xu, Q.; Lu, X.; Zhang, C.-y. A Label-Free Bioluminescent Sensor for Real-Time Monitoring Polynucleotide Kinase Activity. *Anal. Chem.* **2014**, *86*, 8481−8488.
(21) Li, P.-P.; Cao, Y.; Mao, C.-J.; Jin, B.-K.; Zhu, J.-J. TiO2/g-C3N4/CdS Nanocomposite-Based Photoelectrochemical Biosensor for Ultrasensitive Evaluation of T4 Polynucleotide Kinase Activity. *Anal. Chem.* **2019**, *91*, 1563−1570.
(22) Cui, L.; Hu, J.; Li, C.-c.; Wang, C.-m.; Zhang, C.-y. An electrochemical biosensor based on the enhanced quasi-reversible redox signal of prussian blue generated by self-sacrificial label of iron metal-organic framework. *Biosens. Bioelectron.* **2018**, *122*, 168−174.
(23) Zhang, G.; Chai, H.; Tian, M.; Zhu, S.; Qu, L.; Zhang, X. Zirconium−Metalloporphyrin Frameworks−Luminol Competitive Electrochemiluminescence for Ratiometric Detection of Polynucleotide Kinase Activity. *Anal. Chem.* **2020**, *92*, 7354−7362.
(24) Gu, C.; Gai, P.; Han, L.; Yu, W.; Liu, Q.; Li, F. Enzymatic biofuel cell-based self-powered biosensing of protein kinase activity and inhibition via thiophosphorylation-mediated interface engineering. *Chem. Commun.* **2018**, *54*, 5438−5441.
(25) Li, M.; Lv, M.; Wang, L.; Fan, C.; Zuo, X. Engineering electrochemical interface for biomolecular sensing. *Curr. Opin. Electrochem.* **2019**, *14*, 71−80.
(26) Lin, M.; Song, P.; Zhou, G.; Zuo, X.; Aldalbahi, A.; Lou, X.; Shi, J.; Fan, C. Electrochemical detection of nucleic acids, proteins, small molecules and cells using a DNA-nanostructure-based universal biosensing platform. *Nat.Protoc.* **2016**, *11*, 1244−1263.
(27) Kelley, S. O.; Mirkin, C. A.; Walt, D. R.; Ismagilov, R. F.; Toner, M.; Sargent, E. H. Advancing the speed, sensitivity and accuracy of biomolecular detection using multi-length-scale engineering. *Nat. Nano.* **2014**, *9*, 969−980.
(28) Xiao, M.; Lai, W.; Man, T.; Chang, B.; Li, L.; Chandrasekaran, A. R.; Pei, H. Rationally Engineered Nucleic Acid Architectures for Biosensing Applications. *Chem. Rev.* **2019**, *119*, 11631−11717.
(29) Zhang, Q.; Li, X.; Li, B.; Yin, H.; Ai, S. An electrochemical biosensor for the activity assay of polynucleotide kinase and inhibitor screening. *Anal. Methods* **2015**, *7*, 9984−9991.
(30) Song, Z.; Li, Y.; Teng, H.; Ding, C.; Xu, G.; Luo, X. Designed zwitterionic peptide combined with sacrificial Fe-MOF for low fouling and highly sensitive electrochemical detection of T4 polynucleotide kinase. *Sens. Actuators B Chem.* **2020**, *305*, 127329.
(31) Cui, L.; Li, Y.; Lu, M.; Tang, B.; Zhang, C.-y. An ultrasensitive electrochemical biosensor for polynucleotide kinase assay based on gold nanoparticle-mediated lambda exonuclease cleavage-induced signal amplification. *Biosens. Bioelectron.* **2018**, *99*, 1−7.
(32) Fan, C.; Plaxco, K. W.; Heeger, A. J. Electrochemical interrogation of conformational changes as a reagentless method for the sequence-specific detection of DNA. *Proc. Natl. Acad. Sci. U. S. A.* **2003**, *100*, 9134−9137.
(33) Lai, R. Y.; Lagally, E. T.; Lee, S.-H.; Soh, H. T.; Plaxco, K. W.; Heeger, A. J. Rapid, sequence-specific detection of unpurified PCR amplicons via a reusable, electrochemical sensor. *Proc. Natl. Acad. Sci. U. S. A.* **2006**, *103*, 4017−4021.
(34) Kang, D.; Vallée-Bélisle, A.; Porchetta, A.; Plaxco, K. W.; Ricci, F. Re-engineering Electrochemical Biosensors To Narrow or Extend Their Useful Dynamic Range. *Angew. Chem., Int. Ed.* **2012**, *51*, 6717−6721.
(35) Li, H.; Li, S.; Dai, J.; Li, C.; Zhu, M.; Li, H.; Lou, X.; Xia, F.; Plaxco, K. W. High frequency, calibration-free molecular measurements in situ in the living body. *Chem. Sci.* **2019**, *10*, 10843−10848.
(36) Li, C.; Hu, X.; Lu, J.; Mao, X.; Xiang, Y.; Shu, Y.; Li, G. Design of DNA nanostructure-based interfacial probes for the electrochemical detection of nucleic acids directly in whole blood. *Chem. Sci.* **2018**, *9*, 979−984.
(37) Xiao, Y.; Lou, X.; Uzawa, T.; Plakos, K. J. I.; Plaxco, K. W.; Soh, H. T. An Electrochemical Sensor for Single Nucleotide Polymorphism Detection in Serum Based on a Triple-Stem DNA Probe. *J. Am. Chem. Soc.* **2009**, *131*, 15311−15316.
(38) Wu, Y.; Lai, R. Y. Effects of DNA Probe and Target Flexibility on the Performance of a "Signal-on" Electrochemical DNA Sensor. *Anal. Chem.* **2014**, *86*, 8888−8895.
(39) Kékedy-Nagy, L.; Shipovskov, S.; Ferapontova, E. E. Effect of a Dual Charge on the DNA-Conjugated Redox Probe on DNA Sensing by Short Hairpin Beacons Tethered to Gold Electrodes. *Anal. Chem.* **2016**, *88*, 7984−7990.
(40) Lin, M.; Wen, Y.; Li, L.; Pei, H.; Liu, G.; Song, H.; Zuo, X.; Fan, C.; Huang, Q. Target-Responsive, DNA Nanostructure-Based E-DNA Sensor for microRNA Analysis. *Anal. Chem.* **2014**, *86*, 2285−2288.
(41) Deng, M.; Li, M.; Li, F.; Mao, X.; Li, Q.; Shen, J.; Fan, C.; Zuo, X. Programming Accessibility of DNA Monolayers for Degradation-Free Whole-Blood Biosensors. *ACS Mater. Lett.* **2019**, *1*, 671−676.
(42) Peng, G.; Li, X.; Cui, F.; Qiu, Q.; Chen, X.; Huang, H. Aflatoxin B1 Electrochemical Aptasensor Based on Tetrahedral DNA Nanostructures Functionalized Three Dimensionally Ordered Macroporous MoS2−AuNPs Film. *ACS Appl. Mater. Interfaces* **2018**, *10*, 17551−17559.
(43) Su, S.; Xu, Y.; Sun, Q.; Gu, X.; Weng, L.; Wang, L. Noble metal nanostructure-decorated molybdenum disulfide nanocomposites: synthesis and applications. *J. Mater. Chem. B* **2018**, *6*, 5323−5334.
(44) Liu, L.; Zhu, S.; Wei, Y.; Liu, X.; Jiao, S.; Yang, J. Ultrasensitive detection of miRNA-155 based on controlled fabrication of AuNPs@MoS2 nanostructures by atomic layer deposition. *Biosens. Bioelectron.* **2019**, *144*, 111660.
(45) Su, S.; Sun, H.; Cao, W.; Chao, J.; Peng, H.; Zuo, X.; Yuwen, L.; Fan, C.; Wang, L. Dual-Target Electrochemical Biosensing Based on DNA Structural Switching on Gold Nanoparticle-Decorated MoS2 Nanosheets. *ACS Appl. Mater. Interfaces* **2016**, *8*, 6826−6833.
(46) Su, S.; Sun, Q.; Wan, L.; Gu, X.; Zhu, D.; Zhou, Y.; Chao, J.; Wang, L. Ultrasensitive analysis of carcinoembryonic antigen based on MoS2-based electrochemical immunosensor with triple signal amplification. *Biosens. Bioelectron.* **2019**, *140*, 111353.
(47) Zou, H. L.; Li, B. L.; Luo, H. Q.; Li, N. B. 0D-2D heterostructures of Au nanoparticles and layered MoS2 for simultaneous detections of dopamine, ascorbic acid, uric acid, and nitrite. *Sens. Actuators B Chem.* **2017**, *253*, 352−360.
(48) Su, S.; Zhang, C.; Yuwen, L.; Chao, J.; Zuo, X.; Liu, X.; Song, C.; Fan, C.; Wang, L. Creating SERS Hot Spots on MoS2 Nanosheets with in Situ Grown Gold Nanoparticles. *ACS Appl. Mater. Interfaces* **2014**, *6*, 18735−18741.
(49) Lin, M.; Yi, X.; Huang, F.; Ma, X.; Zuo, X.; Xia, F. Photoactivated Nanoflares for mRNA Detection in Single Living Cells. *Anal. Chem.* **2019**, *91*, 2021−2027.
(50) Lin, M.; Wang, J.; Zhou, G.; Wang, J.; Wu, N.; Lu, J.; Gao, J.; Chen, X.; Shi, J.; Zuo, X.; Fan, C. Programmable engineering of a biosensing interface with tetrahedral DNA nanostructures for ultrasensitive DNA detection. *Angew. Chem., Int. Ed.* **2015**, *54*, 2151−2155.
(51) Lin, M.; Yi, X.; Wan, H.; Zhang, J.; Huang, F.; Xia, F. Photoresponsive Electrochemical DNA Biosensors Achieving Various Dynamic Ranges by Using Only-One Capture Probe. *Anal. Chem.* **2020**, *92*, 9963−9970.
(52) Mitsis, P. G.; Kwagh, J. G. Characterization of the interaction of lambda exonuclease with the ends of DNA. *Nucleic Acids Res.* **1999**, *27*, 3057−3063.
(53) Nie, Y.; Yuan, X.; Zhang, P.; Chai, Y.-q.; Yuan, R. Versatile and Ultrasensitive Electrochemiluminescence Biosensor for Biomarker Detection Based on Nonenzymatic Amplification and Aptamer-Triggered Emitter Release. *Anal. Chem.* **2019**, *91*, 3452−3458.

https://dx.doi.org/10.1021/acsami.0c13385
ACS Appl. Mater. Interfaces 2020, 12, 45814−45821

(54) Li, S.; Liao, X.; Mrksich, M. Steady-State of an Enzymatic Reaction is Dependent on the Density of Reactant. *Langmuir* **2013**, *29*, 294−298.
(55) Hou, T.; Wang, X.; Liu, X.; Pan, C.; Li, F. Sensitive electrochemical assay for T4 polynucleotide kinase activity based on dual-signaling amplification coupled with exonuclease reaction. *Sens. Actuators B Chem.* **2014**, *202*, 588−593.
(56) Xu, J.; Gao, Y.; Li, B.; Jin, Y. Cyclic up-regulation fluorescence of pyrene excimer for studying polynucleotide kinase activity based on dual amplification. *Biosens. Bioelectron.* **2016**, *80*, 91−97.

https://dx.doi.org/10.1021/acsami.0c13385
ACS Appl. Mater. Interfaces 2020, 12, 45814−45821